Available online at www.sciencedirect.com
ScienceDirect
Journal of Solid State Chemistry 181 (2008) 735–740
JOURNAL OF SOLID STATE CHEMISTRY
www.elsevier.com/locate/jssc

Facile synthesis of iron oxide with wormlike morphology and their application in water treatment

Lijuan Wan[a,b], Keying Shi[a], Xiqiang Tian[a], Honggang Fu[a,b,*]

[a]*Laboratory of Physical Chemistry, School of Chemistry and Materials Science, Heilongjiang University, Harbin 150080, China*
[b]*Department of Applied Chemistry, Harbin Institute of Technology, Harbin 150001, China*

Received 7 November 2007; received in revised form 1 January 2008; accepted 6 January 2008
Available online 17 January 2008

Abstract

A novel and facile synthesis route for the manufacture of transparent and uniform nanocrystalline α-Fe_2O_3 (nc-Fe_2O_3) thin films and equivalent powders with wormlike morphology is reported, utilizing ferric nitrate as the inorganic source and triblock copolymer as the wormlike morphology-directing agent through the evaporation-induced assembly (EIA) method. X-ray powder diffraction (XRD), ellipsometry, thermogravimetry–differential scanning calorimetry (TG–DSC), Raman spectrum, N_2-sorption and scanning electron microscopy (SEM) were used to study the nc-Fe_2O_3 thin films and powders obtained by calcination at different temperatures. The nc-Fe_2O_3 powder samples showed an excellent ability to remove heavy metal ion (Cr(VI)) in water treatment. The possible formation mechanism of the nc-Fe_2O_3 with wormlike morphology was discussed.

Keywords: Morphology; Evaporation-induced assembly (EIA); Iron oxide; Wormlike

1. Introduction

Among transition metal oxides, iron oxides represent a particularly important class of materials that can be used in a wide range of applications, including catalysis, magnetic devices and rechargeable lithium batteries [1–3]. They combine functionality with low cost and low toxicity. Furthermore, interest in hematite (α-Fe_2O_3) has increased owing to its catalytic and sensory activity, magnetic property [4] and use in water treatment [5]. For all of the applications in various fields, α-Fe_2O_3 thin films or powders with high porosity are desirable.

Transition metal oxides with different kinds of morphologies have been synthesized through chemical or electrochemical methods [6–8]. Contrary to traditional bulk metal oxides, it has proved more difficult to synthesize transition metal oxide homogeneous thin films or powders in the form of high-porosity morphology, owing to the difficulty in controlling the fast rate of reaction. Generally, wormlike nc-Fe_2O_3 thin films could not be directly obtained via conventional synthesis routes, such as the chemical vapor deposition (CVD) method, the sol–gel method, etc. [9–11]. Such effects limit the potential applications of wormlike nc-Fe_2O_3.

Based on the above facts, in order to decrease the hydrolysis rate of the inorganic species, we design a one-step synthesis route through the evaporation-induced assembly (EIA) method, and elucidate the reaction processes leading to the formation of homogeneously wormlike iron oxide thin films. As we know, α-Fe_2O_3 thin films or powders with wormlike morphology has not been synthesized through the facile EIA method so far. We used non-ionic amphiphilic triblock copolymer Pluronic F127 as the morphology-directing agent, which can be easily obtained commercially, and ferric nitrate as the inorganic precursor.

The unique feature of the EIA approach is that this novel strategy combines sol–gel dip-coating and organic–inorganic cooperative assembly techniques. In our strategy, the key step of the system is the action of $NH_3 \cdot H_2O$ and surfactant. The surfactant can be first mixed with

*Corresponding author at: Laboratory of Physical Chemistry, School of Chemistry and Materials Science, Heilongjiang University, Harbin 150080, China. Fax: +86 451 86673647.
E-mail address: fuhg@vip.sina.com (H. Fu).

0022-4596/$ - see front matter © 2008 Elsevier Inc. All rights reserved.
doi:10.1016/j.jssc.2008.01.019

$NH_3 \cdot H_2O$, and then the hydrogen bond may be formed between the hydrophilic block (uncharged water-soluble moieties) and $NH_3 \cdot H_2O$ to decrease the OH^- in the reaction solution. The ferric precursors can hydrolyze slowly to provide relatively smaller inorganic species rather than bulk sediment, which can have a strong interaction with surfactant micelles. At the following stage, the interaction can restrain the transformation from wormlike to bulk morphology when the surfactant is removed.

Chromium has been placed on the top of the priority list of toxic pollutants by the USEPA and is present in aqueous system in both the trivalent form (Cr^{3+}) and hexavalent form (Cr^{6+}). With its high solubility, Cr(VI) is more harmful to living organisms compared to Cr(III) [12]. So the removal capacities of the Cr(VI) ion of the calcined powder samples are investigated. Removal of the adsorbents calcined at different temperatures by a magnet is investigated. The synthesis and characterization of uniform nc-Fe_2O_3 thin films or powders prepared at different temperatures are presented, the formation mechanism of uniform nc-Fe_2O_3 films is discussed, and the water treatment measurements are presented.

2. Experimental

2.1. Materials

Triblock copolymer Pluronic F-127 ($EO_{106}PO_{70}EO_{106}$, MW = 12 600, Product no. P2443-250G) was purchased from Aldrich and used as received without further purification.

2.2. Synthesis of wormlike nc-Fe_2O_3

Isotropic solutions were prepared by dissolving Fe $(NO_3)_3 \cdot 9H_2O$ (4.57 g) precursor and block copolymer F-127 ($EO_{106}PO_{70}EO_{106}$) (0.9 g) in EtOH (23 ml) and H_2O (20 ml; 4.5 ml 26–28% $NH_3 \cdot H_2O$). The solution was refluxed for 1 h. Then they were aged for 24 h at 20–22 °C at ambient environment. Uniform thin films were prepared by dip-coating ITO glass substrates at a constant withdrawal rate (1 mm s^{-1}) and relative humidity (50–60%). Alternatively, the sol solutions can be dried to prepare equivalent iron oxide powders. To remove by-products (ammonium nitrate), powder samples were washed with water. The as-prepared layers or powders were calcined at different temperatures for 4 h (1 °C min^{-1} under air).

2.3. Water treatment experiments

Commercial α-Fe_2O_3 nanoparticle powder was purchased from Beijing Chemicals Co. (Beijing, China). For the experiment, $K_2Cr_2O_7$ was used as the source of Cr(VI), and 0.05 g adsorbent samples were stirred in 25 ml solution containing Cr(VI) for 3 h at room temperature (20 °C). Then the solid and liquid were separated and the concentration of chromium in the remaining solution was measured. For desorption, Cr-loaded iron oxides were shaken with 5 ml of 0.01 M NaOH for 24 h and the particles were separated. The initial concentration of Cr(VI) was 10.80 mg l^{-1}.

2.4. Characterization

Wide-angle X-ray diffraction (XRD) patterns of the iron oxide powder to identify the crystalline phase were recorded on a Rigaku D/max-IIIB (40 kV, 30 mA) diffractometer, using Cu $K\alpha$ radiation with a wavelength of $\lambda = 1.5406$ Å at room temperature. N_2-sorption isotherms of the iron oxide powders obtained on a Micromeritics ASAP 2020 instrument and Brunauer–Emmett–Teller (BET) equation were used to calculate the specific surface area. Thermogravimetry–differential scanning calorimetry (TG–DSC) curves were performed using a NETZSCH STA449C thermal analyzer (1 °C min^{-1} under air atmosphere). Raman spectrum was collected at a HORIBA JY HR 800 spectrometer with a wavelength of $\lambda = 458$ nm (100×, 20 mW). The film thickness was estimated by ellipsometry experiments carried out on a SENTECH GmbH/SE400 instrument with a He–Ne laser beam ($\lambda = 632.8$ nm). Atomic absorption spectra to identify the concentration of Cr(VI) were obtained at a Thermo Elemental SOLAAR-M spectrometer with a wavelength of $\lambda = 357.9$ nm. The morphologies of the calcined iron oxide thin films were evaluated by a Hitachi S-4800 Scanning Electron Microscope with an operating voltage of 20 kV.

3. Results and discussions

3.1. Characterization of iron oxides

Wide-angle XRD was used to identify the crystalline phase of the calcined samples and the results are presented in Fig. 1. As shown in Fig. 1, Bragg diffraction peaks in the

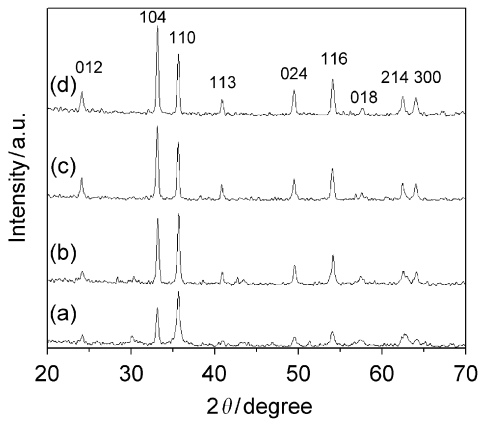

Fig. 1. X-ray powder diffraction patterns of the samples calcined at different temperatures: (a) 350; (b) 400; (c) 450; (d) 500 °C. The XRD patterns are offset for clarity, but the intensity scale is identical for all patterns. I: intensity in arbitrary units.

range $2\theta = 20–70^\circ$, which can be indexed as (012), (104), (110), (113), (024), (116), (018), (214) and (300), show the typical patterns of an α-Fe_2O_3 structure (JCPDF 33–0664) for these samples calcined at 350–500 °C. In Fig. 1, the unindexed peaks (such as ~30) for samples calcined at 350 and 400 °C may be induced by small amounts of impurities. The reason for the existence of small amount of impurities may be incomplete oxidation under relatively low calcination temperature. The crystal size is determined from the broadening of corresponding X-ray spectral peaks by Scherrer's formula as follows: $D = K\lambda/(\beta_c - \beta_s)\cos\theta$, where λ is the wavelength of the X-ray radiation, D is the crystal size, and β_c and β_s are the full-width at half-maximum height of the sample and standard (single-crystal silicon), respectively. With the increase of calcination temperature, these diffraction peaks became more narrow and intense. The average crystallite sizes of the calcined samples estimated from the Scherrer equation using the (104) diffraction peak are summarized in Table 1. As calculated from the Scherrer equation using the (104) diffraction peak of α-Fe_2O_3 for samples calcined at 350, 400, 450 and 500 °C, the average crystallite size was found to be between 17.36 and 33.57 nm. A similar result was found for the (110) diffraction peak. It was found that there is a pronounced increase in the crystal size as the calcination temperature increases, which can be attributed to the growth of crystallites and improvement of crystallization with the increase of calcination temperature. An enhancement of the crystallinity goes in parallel with the aggregation of Fe_2O_3 crystallites as the sintering temperature is increased. This tendency is confirmed by the direct observation of the XRD patterns, where the peak intensity increases and the width of the diffraction peaks becomes narrower with increasing temperature. The crystallite size estimated by applying the Scherrer equation could be somewhat overestimated because of additional microstrain factors [13].

Nanocrystalline Fe_2O_3 (nc-Fe_2O_3) can be applied in magnetic resonance imaging, catalysis, coatings and gas-sensor devices [14]. The BET surface areas of nc-Fe_2O_3 calcined at different temperature are also listed in Table 1. An observed trend is the decrease of BET surface area with the increase of calcination temperature, which is partially attributed to the growth of crystallite size or the particle stacking. Because there are pores between the wormlike Fe_2O_3 nanocrystalline particles and pores may collapse when the particles grow, the decrease of porosity can also induce the decrease of BET surface area.

To further characterize the calcined nc-Fe_2O_3 thin films synthesized at different calcination temperatures, the thickness of the obtained films was determined by using an optical ellipsometer, and the results obtained are listed in Table 1. It is clearly seen that the film thickness is slightly increased as the calcination temperature is increased. This can be ascribed to the growth of crystallites and improvement of crystallization with the increase of calcination temperature.

The Raman spectrum of the sample calcined at 400 °C is shown in Fig. 2. The Raman spectrum peaks observed are four optical modes of even symmetry ($1A_{1g} + 3E_g$), which are expected in the Raman spectrum of α-Fe_2O_3 [15]. Although there are unindexed peaks for the sample calcined at relatively low temperature, no unambiguous signals from other phases are observed. The α-Fe_2O_3 phase is consistent with the results obtained from the XRD analysis. The TG–DSC curves of the as-prepared sample

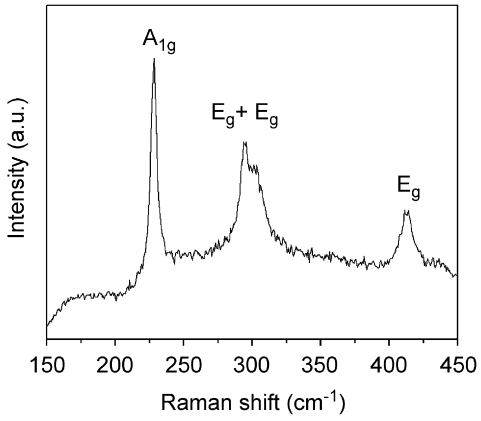

Fig. 2. Raman spectrum of the sample calcined at 400 °C.

Table 1
Textural and structural parameters of wormlike nc-Fe_2O_3 samples and their removal capacity for Cr compared with commercial α-Fe_2O_3

Sample	Crystallite size (nm)[a]	BET surface area ($m^2\,g^{-1}$)	Film thickness (nm)[b]	Removal capacity for Cr [mg g (Cat.)$^{-1}$][c]	Phase
S-350[d]	17.36	45.11	360.5	5.03	α-Fe_2O_3
S-400	26.54	31.62	366.1	4.82	α-Fe_2O_3
S-450	30.64	21.91	368.4	4.35	α-Fe_2O_3
S-500	33.57	20.08	370.1	4.30	α-Fe_2O_3
Commercial Fe_2O_3		2.00		0.70	α-Fe_2O_3

[a]The average crystallite size of α-Fe_2O_3 was calculated by applying the Scherrer equation using the (104) diffraction peak.
[b]The film thickness was estimated by ellipsometry. Film thickness measurement was carried out thin-film samples and other measurements on powder samples.
[c]The removed quality of Cr quality by every gram of the catalyst.
[d]Calcination temperature (°C).

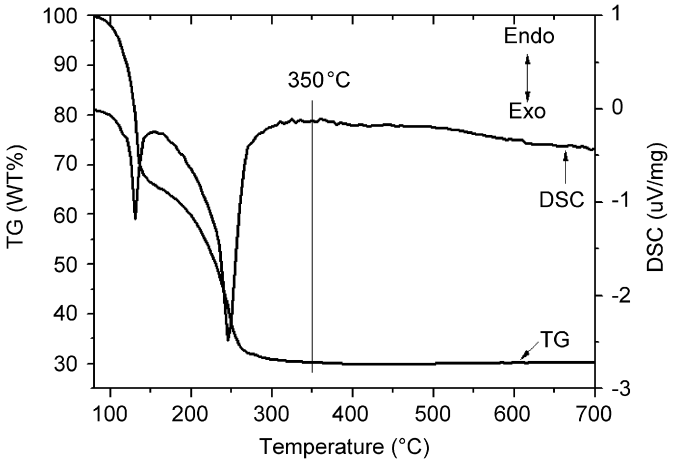

Fig. 3. The TG–DSC curves of the as-prepared sample.

are shown in Fig. 3. From the results of TG–DSC curves, the proper calcination temperature can be measured. It can be seen that the main decomposed temperature of the surfactant is about 245 °C. There is no gravity loss when the temperature is raised to 350 °C, which proves that the organic materials have been removed completely. No carbon stretch or vibration peak is observed from the FT-IR spectrum (Fig. S1), which is further proved by the complete removal of surfactant. The FT-IR spectrum of sample iron oxide is characterized with the IR bands at 547 and 466 cm^{-1}, and this spectrum can be ascribed to the study by Iglesias and Serna [16], which published IR spectra of α-Fe_2O_3 particles of different shapes. For example, α-Fe_2O_3 spheres showed IR bands at 575, 485, 385 and 360 cm^{-1}, while α-Fe_2O_3 laths showed IR bands at 650, 525, 440 and 300 cm^{-1}.

The scanning electron microscopy (SEM) images of our obtained calcined nc-Fe_2O_3 thin films are shown in Fig. 4. From the SEM images, it can be observed clearly that the Fe_2O_3 nanoparticles have typical wormlike morphology. The photograph of transparent and homogeneous thin film and powders are shown in Fig. S2. Evidently, our proposed EIA synthetic strategy is unique in permitting a systematic and facile synthesis of uniform nc-Fe_2O_3 thin films with wormlike nanosize α-Fe_2O_3 by using Fe $(NO_3)_3$ as the inorganic precursor and F127 as the wormlike-structure-directing agent.

3.2. Formation mechanism

On the basis of the above discussion, in an F127-$NH_3 \cdot H_2O$–EtOH-$Fe(NO_3)_3$–H_2O system, the wormlike nc-Fe_2O_3 thin films or powders have been successfully synthesized. It is well known that, in a ternary triblock copolymer–water-selective solvent system, block copolymers can self-assemble into a variety of lyotropic liquid crystal microstructures consisting of a lamellar, hexagonal or cubic structure, with a one-, two-, or three-dimensional order, respectively [17–19]. The very rich structural polymorphism of block copolymer in a ternary system

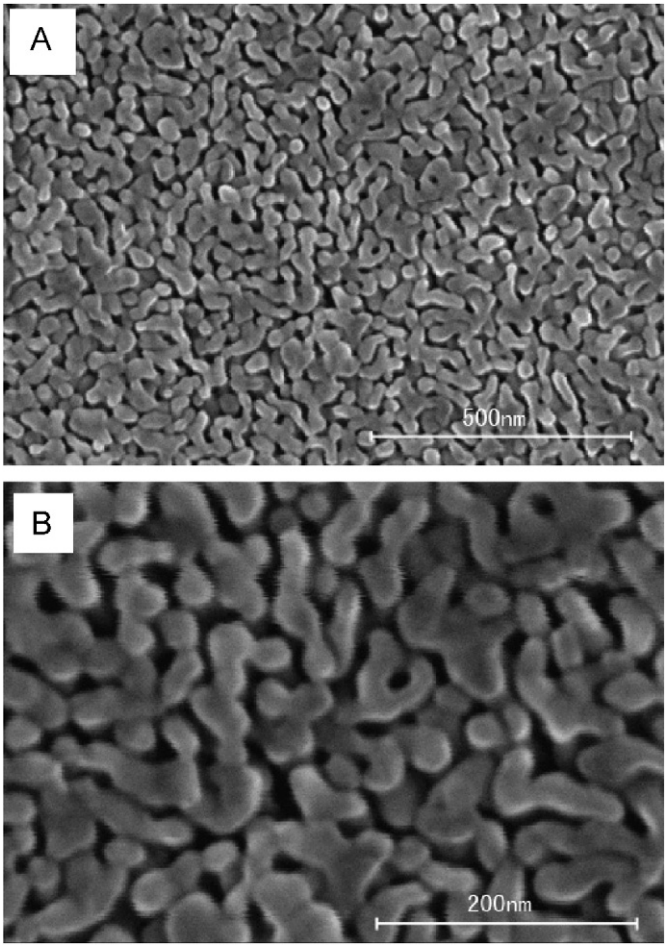

Fig. 4. Representative SEM images at two different magnifications of the nc-Fe_2O_3 thin film calcined at 500 °C for 4 h: (A) lower-magnification SEM image and (B) higher-magnification SEM image.

makes it possible to synthesize wormlike nanostructured films through organic–inorganic cooperative assembly.

The formation of nc-Fe_2O_3 with a wormlike morphology can be attributed to the interaction between the uniform-structure-directing agent (F127) and the hydrophilic ferric nanoclusters and the formation of a surfactant–nanocluster hybrid. A proposed formation mechanism of wormlike nc-Fe_2O_3 through the EIA synthetic route is described in Scheme 1. We believe that there are two factors that influence the synthesis of iron oxides with high porosity as other transition metal oxides. Firstly, it is owing to the strong interplay and the gelation tendency inside the precursors themselves when they hydrolyze. Secondly, the conformation of the crystal phase and the removal of the template under calcination can potentially disrupt the pores between the nanoparticles and form bulk powders.

In our synthetic route, the $NH_3 \cdot H_2O$ first dispersed in the surfactant solution in order to control the rate and prevent the formation of bulk precipitation. The inorganic precursors may hydrolyze slowly, which can have strong interaction with surfactant micelles in the next stage to prevent the pores from collapsing when the surfactant was removed. The reason for the slow hydrolysis velocity of

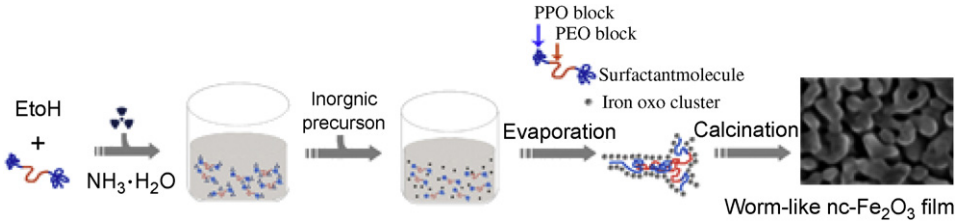

Scheme 1. Schematic illustration of the proposed EIA synthetic approach for the preparation of the nanocrystalline wormlike iron oxide thin films presented in this work.

inorganic species, we suppose, is the weak interaction of the hydrogen bond between the H atom of the $NH_3 \cdot H_2O$ and the O atom of EO of the surfactant, which controls the ionization rate of $NH_3 \cdot H_2O$. Because reaction probability among the inorganic precursors and OH^- in the reaction solution is reduced (i.e. the hydrolysis rate is slowed down), small ferric oxo-clusters, but not bulk sediment, can be obtained. Such ferric oxo-clusters can realize the assembly with the surfactant. We chose the proper quantity of $NH_3 \cdot H_2O$ according to the phenomena of experiments. Only when the solution of surfactant and $NH_3 \cdot H_2O$ became clear, the ferric salt solution could be added. If $NH_3 \cdot H_2O$ was added in the last step, the product was bulk sediment (Fig. S3). Finally, with the evaporation of the volatile solvent, the assembly of the surfactant with the inorganic species and the further cross-link of the inorganic precursors result in the final formation of nc-Fe_2O_3 with wormlike morphology.

The novel EIA synthetic approach allows the process to modulate between solvent removal and inorganic condensation. The products obtained in this synthesis are the aggregates of inorganic ferric oxide particles. The role of F127 is to modify the morphology. Considering the environmental and economic factors, the wormlike iron oxide made from inorganic salts in contrast to ferric alkoxides precursors seems more attractive candidates for potential applications in catalysis and other material applications.

3.3. Water treatment measurement

Herein, we utilized iron oxides powders calcined at different temperatures to investigate their applications in water (containing Cr(VI) ions) treatment. Chromium is considered as one of the primary highly toxic pollutants in water resources and its efficient removal from water is of great importance. For the removal of the metal and anionic contaminant, the mechanism was proposed to involve ion exchange and surface complexation between the iron oxide surface and the toxic ions in the aqueous solution [20,21]. We also investigated the removal ability of commercial α-Fe_2O_3 powder under the same experimental conditions. It was found that the removal ability of wormlike nc-Fe_2O_3 was much better than that of commercial iron oxide (Table 1). The better performances could be attributed to the relatively higher surface area and porous structure of the prepared iron oxides. Powder samples calcined at relatively low temperatures (350 and 400 °C) were observed to be attracted by an outer magnet (Fig. S4). While for powder samples calcined at 450 and 500 °C, no attraction by an outer magnet was observed (Fig. S5). For the sample calcined at 350 °C, such phenomena may be induced by small amounts of impurities and weak ferromagnetism at room temperature due to size effects [22]. For the sample calcined at 400 °C, such phenomena may be induced by small amounts of impurities. Further studies are required to understand this better. The primary objective of desorption is to restore the adsorption capacity of the exhausted adsorbent, while the secondary objective is to recover metals present in the adsorbed phase. The recovered high concentration of Cr(VI) solutions may be thus be considered for recycling in some industrial purposes.

4. Conclusion

In summary, transparent nc-Fe_2O_3 thin films on ITO glass substrates or powders were successfully synthesized by using ferric nitrate as the inorganic source and triblock copolymer F127 as the wormlike-structure-directing agent through a novel and facile EIA approach. With the increase of calcination temperature, the BET surface area of the samples reduced and the particle size and the film thickness increased. We propose that the cooperative assembly between organic and inorganic components results in the formation of wormlike nc-Fe_2O_3 thin films with narrow crystal size distribution. The presence of a copolymer is necessary to produce crack-free films. The wormlike nc-Fe_2O_3 powders at different calcination temperatures showed an excellent ability to remove heavy metal ion Cr(VI) in water treatment and are expected to be useful in many other applications (e.g. catalysis) compared to the traditional Fe_2O_3 powders.

Most importantly, we have demonstrated that, using this route, the hydrolysis rate of the inorganic species can be effectively controlled, and such a simple route may be used for the synthesis of other transition metal oxides with high porosity.

Acknowledgments

The work described in this paper was supported by the Key Program Projects of National Natural Science

Foundation of China (Project no. 20431030), the National Natural Science Foundation of China (nos. 20671032 and 20676027), and the Key Program Projects of Heilongjiang Province Natural Science Foundation of China (no. ZJG0602-01).

Appendix A. Supporting information

Supplementary data associated with this article can be found in the online version at doi:10.1016/j.jssc.2008.01.019.

References

[1] F. Jiao, B. Yue, K.K. Zhu, D.Y. Zhao, H.Y. He, Chem. Lett. 32 (2003) 770–771.
[2] R.F. Ziolo, E.P. Giannelis, B.A. Weinstein, M.P. Ohoro, B.N. Ganguly, V. Mehrotra, M.W. Russell, D.R. Huffman, Science 257 (1992) 219–223.
[3] D. Larcher, C. Masquelier, D. Bonnin, Y. Chabre, V. Masson, J.B. Leriche, J.M. Tarascon, J. Electrochem. Soc. 150 (2003) A133–A139.
[4] (a) D.H. Chen, D.R. Chen, X.L. Jiao, Y.T. Zhao, J. Mater. Chem. 13 (2003) 2266–2270;
(b) M. Pelino, C. Colella, C. Canatalini, M. Faccio, G. Ferri, A. Damico, Sensors Actuators B 7 (1992) 464–469.
[5] L.-S. Zhong, J.-S. Hu, H.-P. Liang, A.-M. Cao, W.-G. Song, L.J. Wan, Adv. Mater. 18 (2006) 2426–2431.
[6] H. Li, R. Liu, R. Zhao, Y. Zheng, W. Chen, Z. Xu, Cryst. Growth Des. 6 (2006) 2795–2798.
[7] L. Suber, P. Imperatori, G. Ausanio, F. Fabbri, H. Hofmeister, J. Phys. Chem. B 109 (2005) 7103–7109.
[8] Y.J. Sun, Y. Chen, L.J. Tian, Y. Yu, X.G. Kong, Q.H. Zeng, Y.L. Zhang, H. Zhang, J. Lumin. 128 (2008) 15–21.
[9] V. Sivakov, C. Petersen, C. Daniel, H. Shen, F. Mücklich, S. Mathur, Appl. Surf. Sci. 247 (2005) 513–517.
[10] S.H. Zhan, D.R. Chen, X.L. Jiao, S.S. Liu, J. Colloid Interface Sci. 308 (2007) 265–270.
[11] S.L. Ren, B. You, J. Du, X.J. Bai, J. Zhang, W. Zhang, A. Hu, B. Zhang, X.X. Zhang, Physica B 400 (2007) 185–189.
[12] J. Hu, I.M.C. Lo, G.H. Chen, Sep. Purif. Technol. 56 (2007) 249–256.
[13] J.B. Cohen, Ultramicroscopy 34 (1990) 41–46.
[14] R.M. Cornell, U. Schwertmann, The Iron Oxides, Wiley-VCH, Weinheim, 1996.
[15] P. Lottici, C. Baratto, D. Bersani, G. Antonioli, A. Montenero, M. Guarneri, Opt. Mater. 9 (1998) 368–372.
[16] J.E. Iglesias, C.J. Serna, Miner. Petrogr. Acta 29A (1985) 363–370.
[17] P. Alexandridis, U. Olsson, B. Lindman, Langmuir 14 (1998) 2627–2638.
[18] P. Alexandridis, U. Olsson, B. Lindman, J. Phys. Chem. B 102 (1998) 1149–1158.
[19] P. Alexandridis, U. Olsson, B. Lindman, Macromolecules 30 (1997) 6788–6797.
[20] M.S. Onyango, Y. Kojima, H. Matsuda, A. Ochieng, J. Chem. Eng. Japan 36 (2003) 1516–1522.
[21] G.A. Waychunas, C.S. Kim, J.F. Banfield, J. Nanoparticle Res. 7 (2005) 409–433.
[22] R.D. Zysler, D. Fiorani, A.M. Testa, L. Suber, E. Agnostinelli, M. Godinho, Phys. Rev. B 68 (2003) 212408.